Topic Title: Image Super Resolution with Coprime Sampling

Student Name: Jinhui Li   **Student ID: z5012918**

A.   Problem statement

As the growing demand for higher signal band- width, it is required to increase the sampling frequency to reach the demand of Nyquist sampling theorem. However, due to the limitations, such as the sensor manufacturing, the size of chips and the price, signal processing algorithms has been applied to get high resolution images from several low-resolution (LR) images.

B.   Objective

Coprime sampling is a very attractive way in the processing of super resolution images, as its low noise ratio. the purpose of this method is to obtain the high resolution images from some aliased low resolution images. Those low resolution images are under-sampled by coprime factor M and N. The coprime sampling algorithm is able to separate the high frequency components from the aliasing.

C.   My solution

Co-prime Sensor Arrays Analysis
Frequency Domain Analysis
Aliasing Separation by Comparing the Down-sampled Images
Frequency Domain Reconstruction and Constructing Super-resolution Image
Enhancement Using Adaptive Steering Kernel Regression

D.   Contributions (at most one per line, most important first)

Implement the Coprime Sampling in High Resolution Algorithms
After process to Improve the Quality
Other Methods of Super Resolution Implementation (NEDI and SCSR)
Comparison of Those Algorithms

E.   Suggestions for future work

Optimizing the Algorithm
After Processing

While I may have benefited from discussion with other people, I certify that this report is entirely my own work, except where appropriately documented acknowledgements are included.

Signature: _____   Date: __Oct./26/2016_____

Pointers

List relevant page numbers in the column on the left. Be precise and selective: Don't list all pages of your report!

1	Problem Statement
1	Objective

Theory (up to 5 most relevant ideas)

9	Interpolation-Based Super Resolution
14	Reconstruction-Based Super Resolution
18	Learning-Based Super Resolution
20	Challenge issues for super-resolution

Method of solution (up to 5 most relevant points)

9	NEDI New Edge Directed Interpolation
14	Non-uniform Interpolation Approach
15	Projection onto Convex Sets Approach (POCS)
16	Statistical Method
18	ScSR Spare Coding super-resolution

Contributions (most important first)

28	Co-prime Sensor Arrays
29	Image Reconstruction
34	Enhancement Using Adaptive Steering Kernel Regression

Results

41	2D Image with coprime sampling
44	The Comparison of Each Pixel
46	The Comparison of Time and PSNR

Conclusion

47	Statement of whether the outcomes met the objectives
47	Suggestions for future research

Literature: (up to 5 most important references)

3	[1] PU J, ZHANG J, HUANG H, 2009.
11	[4] Chen JJ. ,Liang QL. ,Zhang BJ. ,Wu XR., 2013
15	[10] S. Qin, Y. D. Zhang, and M. G. Amin, 2015
25	[17] Yang JC,Wright J,Huang ThS, 2010
33	[19] Takeda H, Farsiu S, Milanfar P, 2007

THE UNIVERSITY OF
NEW SOUTH WALES

SCHOOL OF ELECTRICAL ENGINEERING
AND TELECOMMUNICATION

Image Super Resolution with Coprime Sampling

by

Jinhui Li

Thesis submitted as a requirement for the degree

Master of Engineering (Electrical Engineering)

Abstract

As the growing demand for higher signal band- width, it is required to increase the sampling frequency to reach the demand of Nyquist sampling theorem. However, due to the limitations, such as the sensor manufacturing, the size of chips and the price, signal processing algorithms has been applied to get high resolution images from several low-resolution (LR) images. The purpose is to realize the high-resolution images reconstruction with a higher quality vision effect from one or a lot of low resolution images, which are shot from the same scenery. This article has introduced the origin and concept of super resolution. Some classical algorithms are presented with their characters, including the merits and the problems and the comparison will be given.Coprime sampling is a very attractive way in the processing of super resolution images, as its low noise ratio. the purpose of this method is to obtain the high resolution images from some aliased low resolution images. Those low resolution images are under-sampled by coprime factor M and N. The coprime sampling algorithm is able to separate the high frequency components from the aliasing. It shows that coprime sampling has good detection performance and also reduce the complicity of algorithm and sampling rate. The expected super resolution methods can reconstruct high- frequency components which is otherwise unavailable in the single low resolution image. The effectiveness of this technique will be verified with other methods by comparing the simulation results.

Abbreviations

CSA Co-prime Sensor Array

DOA Direction of Arrival

FIR Finite Impulse Response

MAP Maximum A Posteriori Method

ML Maximum Likelihood

PSNR Peak Signal-to-Noise Ratio

MUSIC Multiple Signal Classification

NEDI New Edge-Directed Interpolation

SCSR Super-Resolution Sparse Representation

SNR Signal-to-Noise Ratio

SR Super Resolution

ULA Uniform Linear Array

POCS Projection onto Convex Sets Approach

Contents

Chapter 1

Introduction

1.1 Super-resolution Images

Super-resolution images are a typical of technique to apply the algorithms in processing one or several images to get the HR image. High resolution means high density of pixels, which is able to provide more detail, and those details play an important role in many areas. The most direct method to compute a high resolution image is using the sensors of high resolution images.

High resolution images or video are often required for the after image processing as well as its analysis. There are two main areas for the high resolution application: improved graphical information for human interpretation and help to represent automatic machine awareness. High resolution images refer to more details existed in the images. The detail will increase along with the improve of resolution. The resolution of the image can be categorized on many different ways, such as the pixel resolutions, temporal resolutions, spectral resolutions, radiometric resolutions and spatial resolution. In most cases, we are mainly concerned with spatial resolution.

The super resolution resolution of the image is first limited within the sensor of the image or the device. There are typically two type of sensors. One is the charge-coupled device (CCD). And another one is the complementary Metal Oxide Semiconductor (CMOS) active pixel sensor. These kind of sensors are located in the two-dimensional array that is typically organized two-dimensional signals. The equivalent number of sensors elements

per unit area of the sensor unit and the size is determined so as to capture the spatial resolution of the first image. High density of the sensor, the possible high spatial resolution of the imaging system. Aliasing in the lower spatial sampling frequency, under-detector imaging system generates a low-resolution image bulk film. A direct method to increase the spatial resolution of the whole image system is changing the density of the sensors and reduce the size of the sensors. Along with the decrease of the size of sensors, the amount of light incident on the respective sensors will cause a so-called shot noise reduction. In addition, the increase in hardware cost density sensor or pixel density of the image corresponding to the sensor is increased. Thus, the size of the sensors play a significant role in increaseing the spatial resolution.

For many digital images applications, the high resolution images or video is often desirable for the after image processing and data analysis. Improved graphical information help to express the human interpretation and automatic machine recognition graphic information. The need for high-resolution images come from two main areas of application. Details of the resolution of the image included in the image detail will be described will be increased with the increase of the detailed resolution. Pixel resolution, time resolution, the spectral resolution of radiation resolution and spatial resolution: the resolution of the digital image can be classified in various ways. If this is primarily related to the spatial resolution.

The image sensor, limiting the spatial resolution of the image view (high frequency band) is also due to (sensor point spread function (PSF) associated with) the lens cloudy, lens aberration effcts diractions the aperture, the optical blur due to the limited movement in the optical. Very high constituting the imaging chip and an optical component that captures an image of the resolution is very high, most of it is not practical in actual application, for example, widely used in monitoring cameras, and that the built-in camera on a mobile phone. In addition to the cost of resolution surveillance camera hardware speed it is limited to storage. In other scenarios, such as satellite imagery to use a di cult resolution sensors by physical constraints. Another way to solve this problem is to use signal processing to create a process to accept the recorded image degradation to replace the hardware cost calculation cost OAE image. This technique is particularly referred to
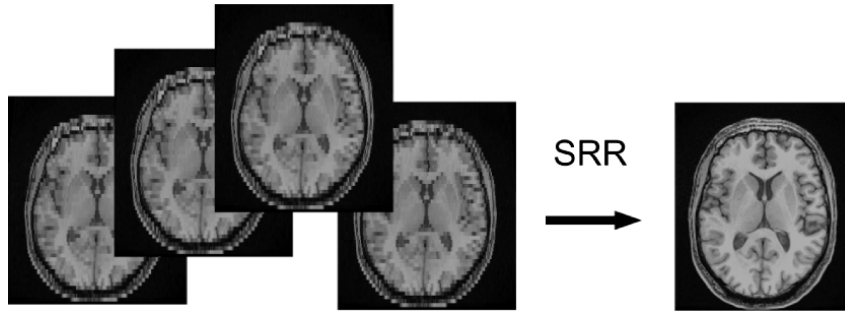
as a reconstruction super resolution (SR).

The super-resolution (SR) is to produce an image of high resolution (HR) image from multiple observed lower resolution (LR)[1], a technique for increasing the performance degradation due to the image processing of the low-resolution camera and a high-frequency component removed. SR is the basic concept of the non-included in the plurality of low resolution frames to produce a high resolution image - to combine the redundant information.

Closely related to the SR techniques are one of an image interpolation method which is applied to increase the pixels of the image. Since there are no more additional information supplied, the quality of the image with interpolation is extremely limited nature of problem raised unjust, it is not possible to recover the frequency components of loss. However, the scheduling settings may be observed multiple low-resolution reconstruction problem is more limited. Non-redundant information contained in these images LR are generally introduced by the sub-pixel shift between them. May result in uncontrolled motion between the imaging system and field because the pixel shift may, for example, due to the movement or control operation of an object, such as satellite imaging system orbiting the earth at a predetermined speed.

However, as the limitation of manufacturing technique and cost, it is unrealistic in many situation and large scale production. Many area are benefit from this, if it is able to apply super-resolution algorithm to compute the HR image . Those approach is the most attractive research area, which refers to super resolution (SR) or high resolution image reconstruction or sometimes called resolution enhancement in [1]. Specifically, to the Social security or terrorism, it is difficult to find the potential threat in the low resolution images or videos. As a result, it is desired to capture the abnormal activities from high resolution technology. Traditional compression has some limitations, if the super-resolution is introduced, the size of image can be reduced before compression, and then recover the image, which means the compression ratio has been improved. In addition,It is pretty helpful for a doctor to make a correct diagnosis if the HR image algorithm can introduced to medical care. It will be easier to detect an object from many similar objects if it is able to get a HR satellite images. Meanwhile, if an HR image is introduced, the

performance of pattern recognition in computer vision can be improved.

Fig. 1.1 Standard clinical magnetic resonance imaging (MRI)

Currently, some researches to the super-resolution image can be classified to 3 class: based on interpolation, reconstruction and learning[2], which will be discussed later.

1.2   Coprime sampling

The signal is sampled from two samplers with the sub-Nyquist sampling rates M and N are coprime integers[3]. In practical application of signal detection, it is required to obtain the a higher sampling frequency, which also has increased the amount of data and bring some problems in the real systems. The coprime sampling, to some extent, is able to solve those problems. Coprime sampling, ensuring the low noise ratio, reduce the requirement of sampling frequency.

Spectral density estimation is to detect the frequency domain in the data. It should be mention in here that if the sampling rate satisfy the Nyquist theorem, the spectral of a signal thus is able to be determined uniquely. However, along with its requirement of high sampling frequency and signal bandwidth, it needs amount of sensors or measurement devices to reach this demand. The coprime sampling is very attractive between many techniques that are available to those kind sampling methods [3]. Coprime sampling was firstly proposed to distinguish the deterministic sinusoids in noise [4]. After that, the relevent robust versions were pointed out [3] due to the existance of noise in processing. The problem is that this algorithm requires a lot of samplers to distinguish the different frequency signals.
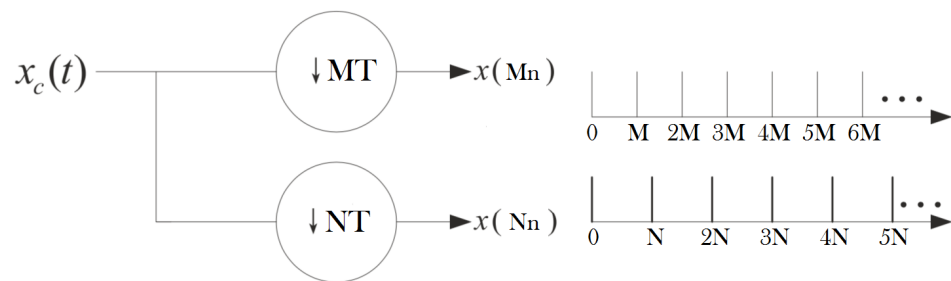
Fig. 1.2 Example of coprime sampling

Chapter 2

Techniques for super-resolution

Based on literatures surveyed, there are several SR algorithms. Those methods are mainly focus on the particular domain, spatial/frequency, and its purpose to solve specific problems.

2.1 Interpolation-Based Super Resolution

Multi-frame super-resolution technology is the most visually method. Firstly, the information of the relative motion among frames is estimated to get the pixel value in the nonlinear space. Then, based on nonlinear interpolation, the value of HR grid will be get. Finally, the technology of image recovery is applied to deblur and reduce the noise. Rajan and Chaudhuri point out the method of general interpolation by 3 steps: decomposition, interpolation and fusion. TAOHJ[2] raised the bilinear interpolation in wavelet domain.

The advantage of those methods is the fast and easy to compute. It is able to satisfy the requirement of real-time. However, owing to the introduction of extra high frequency information, it is hard to get the effect of sharpness.

2.1.1 NEDI New Edge Directed Interpolation

If we consider that without loss of generality, we assumed the image size $X_{i,j}$ a low resolution image of H W coming from the size of $2H * 2W$, i.e. $Y_{2i,2j} = X_{i,j}$. We use the following basic idea of presenting the new interpolation algorithm: interpolating the

interconnection lattice $Y_{2i+1,2j+1}$ which is compute from the lattice $Y_{2i,2j} = X_{i,j}$.

$$\hat{Y}_{2i+1,2j+1} = \sum_{k=0}^{1} \sum_{l=0}^{1} \alpha_{2k+l} Y_{2(i+k),2(j+l)}$$

Here are the closest includes your neighbor interpolation along a diagonal direction. It is assumed that the Gaussian process can modeled the natural inage source.Based on the classical theory (Wiener filter), it is given by the optimal MMSE linear interpolation coefficient

$$\vec{\alpha} = R^{-1}\vec{r}$$

where $R = [R_{kl}], (0 < k, l < 3)$ and $r = [r_k], (0 < k < 3)$ is the partial covariance at the high resolution.

We propose to evaluate a high-resolution coponents from the counterpart of the low-resolution qualitative model, which characterize the relationship between the covariance resolution. After that, we will begin from the step edge in the ideal model for the case of one-dimensional signal(1-D) [18]. The sampling interval of the high resolution to the low local fixed Gaussian is assumed to 2d and d respectively. As a result, the relationship among the normalized covariance sampling interval can then be estimated by the followed equation , $R(x) = e^{-x^2/2\sigma^2}$.

It shows that the covariance of high-resolution can be supposed to the covariance of low-resolution with the quadratic-root function $R(d) = R(2d)^{0.25}$. along with the sampling distance d goes to 0, R(d) can be then described by R(2d) for the computation efficiency.

Regard to a 2-D signal, images in particularly, one signficant factor to the successful alignment is to obtain high-resolution covariance knowledge. Geometrical rule of the edge means the pharmaceutical smoothly with the edge sharpness and pharmaceutical direction over with predefined edge orientation[18]. The direction-related properties of the edge can affect the visual quality of the area around the edges directly. It needs to metioned in here that the local covariance structure contains enough information to estimate the local covariance structure. However, there are some problems. Instead, we estimate the covariance of high resolution from low resolution relative accoding to

the estimated ultimate proposal "geometric duality." Due to limitations of the explicit approach, we do not want to estimate the direction of the local covariance.
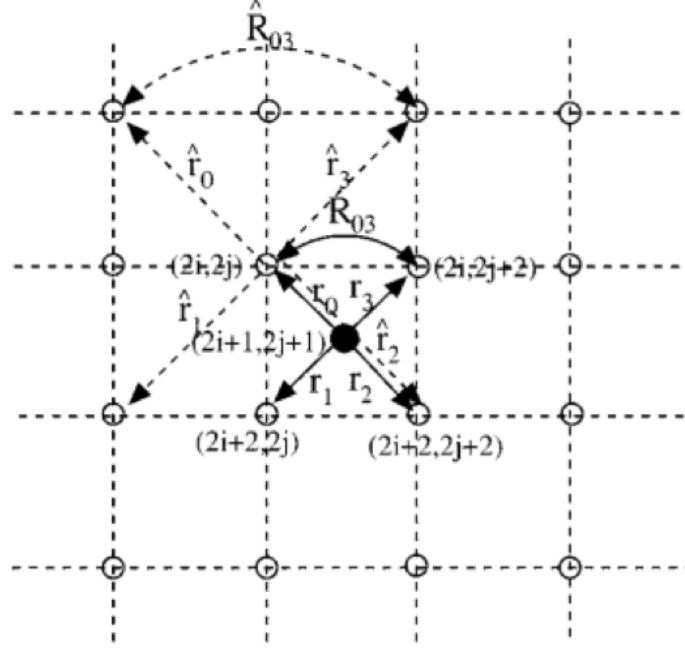
Fig. 2.1 Interpolating from $Y_{2i,2j}$ to $Y_{2i+1,2j+1}$

Geometrical duality can be described as the correspondence among the different resolutions.

The followed figure describes the geometric duality among the high-resolution covariance $R_{k1,rk}$ and the low resolution covariance estimation of $Rk1, rk$ when we interpolate the interlacing lattice $Y_{2i+1,2j+1}$ from $Y_{2i,2j}$. The geometrical duality is to estimate the local covariance for 2-D signals in the local covariance without the need of the edge orientation. Similar geometric duality can also be observed in the followed figure, when the interpolatation is the interlacing lattice $Y_{i,j}$ (i+j = odd number) from the lattice Yi, j (i+j = even number). In fact, both figures are same to the scaling factor of $2^{1/2}$ and the rotation factor of $\pi/4$.

When the estimating a high-resolution and low-resolution covariance covariance response relationships it can directly connect with the existing covariance and covariance estimation method based adaptation measures.

The low-resolution covariance $R_{kl,rk}$ can then be caculated from the local piexels of low resolution images by applying method

$$\hat{R} = \frac{1}{M^2}C^T C, \hat{\vec{r}} = \frac{1}{M^2}C^T \vec{y}$$

where $y = [y_1...y_k...y_{M^2}]^T$ is the signal vector, which contains MxM pixels within the local pixels. Meanwhile, C is the $4 \times M^2$ signal matrix[18]. Its kth column vectors can be represented by the four nearest neighbours of y_k considering the diagonal direction. Then we can get

$$\vec{\alpha} = (C^T C)^{-1}(C^T \vec{y})$$

Covariance based adaptive edge-oriented nature is to adjust the interpolation coefficient and match the random orientation. The more detailed justification real estate in the same direction. However Co. scale can affect (you can usually find in the texture pattern, for example, tightly packed edges), preservation of the true direction of the edge of the sampling frequency of the working class down because of aliasing and edge model[18].
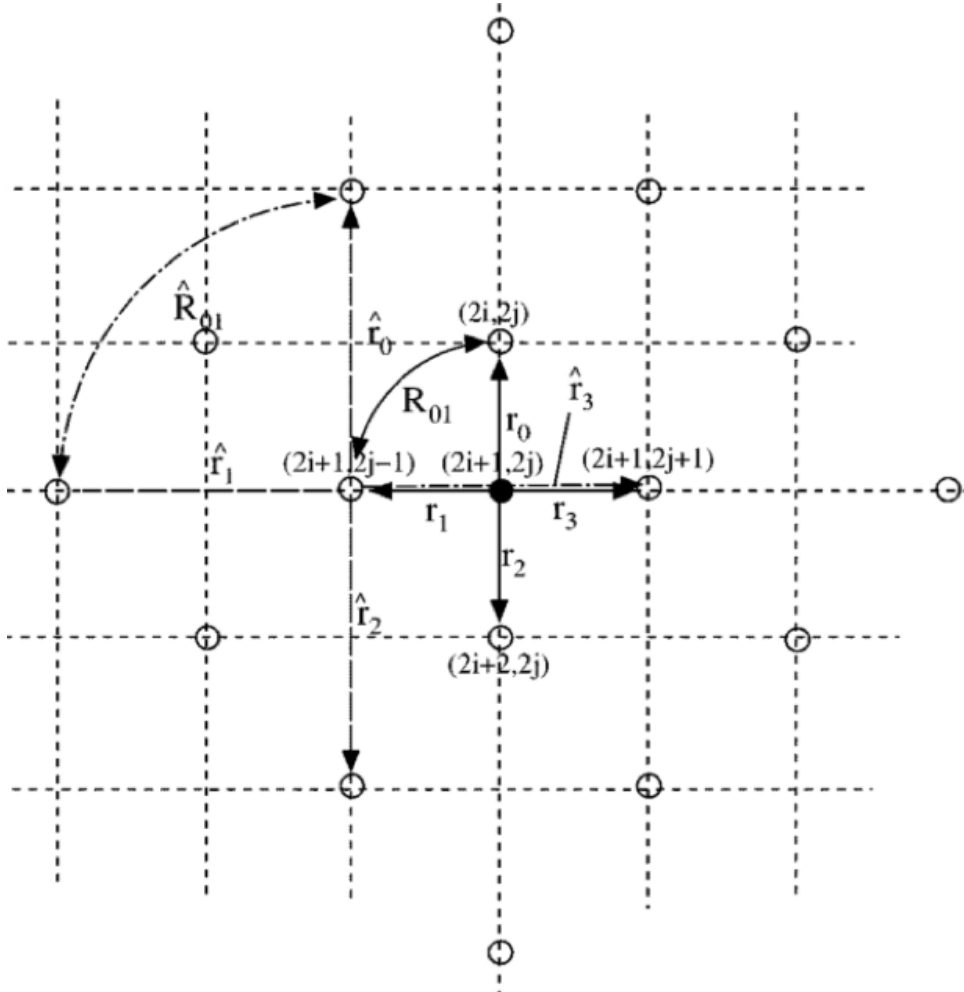
Fig. 2.2 Geometric duality for the interpolation of $Y_{i,j}$(odd numbers) from $Y_{i,j}$ (even numbers)

However, the main drawback of covariance based adaptive interpolation is the computational complexity. If the window size is changed to M=8, the computation requires around 1300 multiplications for each pixel. When we compared with the linear interpolation to be applied when an adaptive interpolation for every pixel based on the covariance, the overall complexity is increased about twice. To reduce the computational complexity, The followed method is introduced. The adaptive interpolation based on the covariance only is applied to the edge pixels (pixels near the edge); For more edge pixels (pixels of the soft zone), we still use a simple linear interpolation. This hybrid system is based on the observation of the pixels are often adapted based on the covariance advantage consists of the small portion of the total image edge pixel edge. Pixels (e.g., four close neighbors from the estimated local distribution) measuring the activity if the preset threshold value Th or more is declared as edge pixels. Owing to the calculation of the activity measurement is usually negligible compared to that of the covariance estimation, it is possible to obtain a small portion of the image containing the complex dramatic decrease edge pixels.

2.2   Reconstruction-Based Super Resolution

This is the most common methods. It is assumed that the image only has some suitable transformation, shift and noise disturbance. There are generally two parts to reconstruct the image: registration and reconstruction. The general methods are application of maximum a posteriori(MAP), iterative back projectim(IBP)[1] and Projection onto Convex Sets Approach(POCS)[2]. Only required some partial priori hypothesis, the effect of blur and aliasing, to some extent, will be reduced.

2.2.1   Non-uniform Interpolation Approach

Ur and Gross [2] searched a non-uniform interpolation of an ensemble of spatially shifted LR images by realising the generalized multi-channel sampling theorem of Papoulis and

Brown. This algorithm is the most visual method for SR image reconstruction. It consists of three steps (as illustrated in followed figure):

1.Registration. It is to estimate the relative motion, if the motion information are unknown.

2. Interpolation. To improve the resolution of the images. Non-uniform interpolation has been applied.

3. De-blurring process. This step is depending on the observation model and previous process.
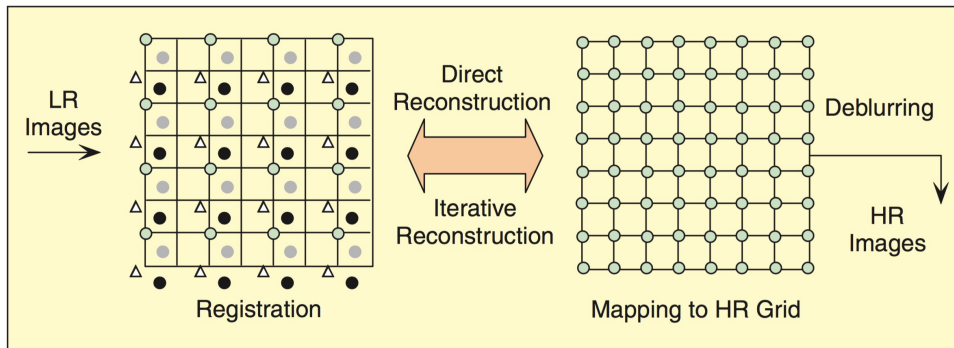
Fig. 2.3 Registration Interpolation based reconstruction

It is proposed a scheme to acquire an improvement resolution image by using the Landweber algorithm from a certain number of images taken with multi-sensors [1]. The block matching method has been employed for determining the relative shifts. However, if the cameras possess the same aperture, there are still some limitations both in its arrangement and configuration.

This difficulty can be solve by multiple cameras with no more than one apertures [1]. The advantages of the non-uniform interpolation method is that it takes lower computational load and able to realize the real-time process. The problem, however, in this method is that the degradation models are limited. It is only practical and realizable when the blur and the noise are similar for the low resolution images. In addition, the optimality of whole reconstruction technique is not guaranteed, beacuse the step of restoration does not consider the errors for the interpolation.

2.2.2 Projection onto Convex Sets Approach (POCS)

POCS algorithm has the good ability to contain spatial prior information, and the ability to integrate the prior information into the reconstruction process. The basic idea is that certain features of the high-resolution images, such as data reliability, energy boundedness and smoothness, is refer to the different convex set of constraints. By using those alternating the role of these projection of the intersection of convex set, it is able to compute the solution to meet all of the constraints convex sets, and realize the high resolution image reconstruction.

Iteration can be taken to compute the initial estimation of x_0, which is the estimated projection of convex sets projection operators P_i, it is able to obtain the desired high-resolution image. The initial estimate x_0 is usually used in interpolation method of constructing a high resolution image, use the constraint set correction x_0 observation sequence until the iteration termination condition is satisfied. By the high-resolution image reconstruction algorithm POCS can be written as

$$\mathbf{x}_{n+1} = P_m P_{m-1} \cdots P_1 \mathbf{x}_n$$

Due to add a variety of convenient ability to maintain a strict priori constraint information, POCS algorithm has been widely applied in practice. However, the result of the reconstruction algorithm depends on the initial estimate, and the convergence of iterative algorithm is slow. In addition, its stability needs to be improved.

Fig. 2.4 Comparison between interpolation and POCS (left: Original Image, Middle: Bilinear interpolation, Right: POCS algorithm)

2.2.3 Statistical method

Statistical method is also known reconstruction method based on probability. Reconstruction algorithm based on probability can be divided into maximum a posteriori method (MAP) and maximum likelihood estimation method (ML). The meaning of maximum a posteriori probability method is the promise of a known sequence of low-resolution images, so that to maximize the posterior probability of a high resolution image. The maximum likelihood probability method can be considered as a special case in any prior model of the maximum a posteriori probability algorithm. The maximum a posteriori method is currently researched widely.

Maximum a posteriori reconstruction algorithm is the low-resolution image reconstruction by the following equation in the observation model to obtain a high resolution original image. It means to get the maximum value of the posterior probability of the original image resolution.

$$\hat{\mathbf{x}} = \arg \max_{\mathbf{x}} \Pr(\mathbf{x} \mid \mathbf{y})$$

Take the Bayes' theorem in here,

$$\hat{\mathbf{x}} = \arg \max_{\mathbf{x}} \frac{\Pr(\mathbf{y} \mid \mathbf{x}) \Pr(\mathbf{x})}{\Pr(\mathbf{y})}$$

As the right side of this equation is irrelative to the denominator, so that we can get

$$\hat{\mathbf{x}} = \arg \max_{\mathbf{x}} \Pr(\mathbf{y} \mid \mathbf{x}) \Pr(\mathbf{x})$$

Thus, the posterior probability of high-resolution image equivalent to the multiplication of prior probability and the conditional probability of the low-resolution images. It is notice in here, that $Pr(y|x)$ is the conditional probability of a low resolution image in the high resolution image which is known. Pr (x) is the prior probability of a high-resolution images, Pr (y) is the posterior probability of a low-resolution image, which is generally considered independent of the solution process. Conditional probability usually use the Gaussian model or Markov model, and prior probability can choose a variety of different models according to different needs, It shown be mention in here that the models generally

should be chosen to maintain the ability to function with convex edges, such as TV model, BTV model. The Fig shows the comparison of MAP and the bilinear interpolation.

Fig. 2.5 Comparison between interpolation and MAP (left: Original Image, Middle: Bilinear interpolation, Right: MAP algorithm)

2.3 Learning-Based Super Resolution

It is based in the image set to calculate the field relationship among the patch of sampling set and the patch of image set. Then, the Optimal weight constraint is constructed, and using the previous process or assumption to get the closest sampling value. When the low resolution cannot provide enough information to reach the demand of high resolution, learning-based methods can obtain more high layer information. Thus, those methods have the huge advantages. It is able to reach the desired results in the super-resolution image applications. It provides some new ideas to reconstruct the high frequency information in the case of large sampling rate.

Chang [1] firstly indicated the neighbor embedding method. It is assumed that the high resolution and the corresponding low resolution images have the same geometry structure. The neighbor embedding method does not require a large number of sampling, and not sensitive to noise.

It also pointed out the hallucination face, which only focus on human face. As the introduce of the pre-assumption, this method has largely improved the quality of image. However, for the more general human face, including the impact of emotion, age and race, this algorithm can only get the 4 times amplifying effect.

2.3.1 ScSR Spare Coding super-resolution

For the given single low-resolution input, and a set of pairs (high- and low-resolution) of training patches sampled from similar images, it is desired to reconstruct a high-resolution version of the input. The advantage of this method is more widely applicable than re-constructive (many image) approaches. However, the difficulty of this method is that the single-image super-resolution is an extremely ill-posed problem[20].

High-resolution patches have a sparse linear representation with respect to an over complete dictionary of patches randomly sampled from similar images.

$$\boldsymbol{x} \approx \boldsymbol{D}_h \boldsymbol{\alpha} \quad \text{for some } \boldsymbol{\alpha} \in \mathbb{R}^K \text{ with} \|\boldsymbol{\alpha}\|_0 \ll K$$

where output high-resolution patch $\boldsymbol{x} \in \mathbb{R}^n$ and high-resolution dictionary $\boldsymbol{D} \in \mathbb{R}^{n \times K}$.

We do not directly observe the high resolution patch , but rather (features of) its low-resolution version. The low-resolution patch in Dl sparse representation will be used to recover the corresponding high-resolution patch from Dh[16].

$$D_l \;=\; L D_h \in R^{d \times n}$$

where L is the down sampling and blurring operator. The input low-resolution patch satisfies

$$\boldsymbol{y} \doteq L\boldsymbol{x} = L\boldsymbol{D}\boldsymbol{\alpha}_0$$

Formally, we seek the sparsest solution:

$$a_0 \;=\; arg\ min\|a\|_0\ \ subj\ \ y \;=\; D_l\, a$$

$$a_1 \;=\; arg\ min\|a\|_1\ \ subj\ \ y \;=\; D_l\, a$$

We can find a sparse representation of the D_l. The D_h generates a high-resolution high-definition output patch base patches corresponding x be combined in accordance with a coefficient. Sparsest problem of finding the expression of y may be formulated as follows:

$$\min \|\boldsymbol{\alpha}\|_0 \quad \text{s.t.} \quad \|F\boldsymbol{D}_l\boldsymbol{\alpha} - F\boldsymbol{y}\|_2^2 \le \epsilon$$

where F is the (linear) the feature extraction operator. The primary role of F is to provide a perceived sense constraints on how closely the coefficient Y approximation[21]. A desired coefficient sufficiently sparse as shown, they suggest that efficient instead be recovered by minimum norm:

$$\min \|\boldsymbol{\alpha}\|_1 \quad \text{s.t.} \quad \|F\boldsymbol{D}_l\boldsymbol{\alpha} - F\boldsymbol{y}\|_2^2 \leq \epsilon$$

Lagrange multipliers offer an equivalent formulation

$$\min_{\boldsymbol{\alpha}} \|F\boldsymbol{D}_l\boldsymbol{\alpha} - F\boldsymbol{y}\|_2^2 + \lambda\|\boldsymbol{\alpha}\|_1$$

The Lagrangian multiplier provides an equivalent formula for the lambda equilibrium solution of the sparsity and approximation of the fidelity of y. Here, F concatenates first and second image partial derivatives, computed from a bicubic interpolation of the low-resolution input. Emphasizes the part of the signal that is most relevant for human perception and for predicting the high-resolution output.

Transforms usual l fidelity criterion into a more perceptually meaningful Mahalanobis distance. Sparsity in fixed bases (wavelet), or learned bases (K-SVD, alternating minimization) has been applied extensively to image compression, denoising, inpainting, and more recently to classification and categorization. For super-resolution, sparse representation in simple bases of randomly sampled patches already performs competitively.The input is training dictionaries D_h and D_l, a low-resolution image Y[20].

For each 3x3 patch of Y, taken staring from upper left corner with 1 pixel overlap in each direction, and then compute the mean pixel value m of patch y. after that, we can solve the optimization problems with the estimated D and y by:

$$\min_{\boldsymbol{\alpha}} \|\tilde{\boldsymbol{D}}\boldsymbol{\alpha} - \tilde{\boldsymbol{y}}\|_2^2 + \lambda\|\boldsymbol{\alpha}\|_1$$

The high-resolution patch can be generated with $x = D_h A*$, and put the patch x+m into a high-resolution image Xo. Using gradient descent, we can find the closest image to X_0 which satisfies the reconstruction constraint

$$\boldsymbol{X}^* = \arg\min_{\boldsymbol{X}} \|SH\boldsymbol{X} - \boldsymbol{Y}\|_2^2 + c\|\boldsymbol{X} - \boldsymbol{X}_0\|_2^2$$

The Super-resolution image X* is achieved.

2.4 Challenge issues for super-resolution

Other algorithm in the SR caculation to improve their performance are focused on the color SR algorithm and the compression algorithm currently. Super-resolution reconstruction technology has already become a hot topic in image processing as its significant meaning in practice. However, there are still many problems need to be solved.

2.4.1 Image Registration

Image registration is an important process based on the multi-frame image reconstruction. The aim is to obtain the sequence of low-resolution image registration information in mutual displacement between the images to realize the further reconstruction. Due to the existence of different sub-pixel displacement between the low-resolution image sequences, it is these sub-pixel level displacement provides complementary information. Therefore, registration accuracy of the results directly affects the reconstruction results. The higher the accuracy of the displacement information can be better anti-aliasing, the effect of image reconstruction to get better. Super-resolution reconstruction of image registration methods should be considered prior knowledge and a variety of unrelated movement during imaging equipment and image capture scenes movement. In addition, consideration should be given image registration process into the super-resolution rate in the reconstruction process, that is, as the reconstruction process changes.

2.4.2 Computation Efficiency

Super-resolution image reconstruction technique applied in practice play an important role. It is necessary to consider each algorithms complexity and speed. The most common case is that the effects of reconstruction algorithms and the speed and complexity of conflicting are always restricted. simple algorithm with the fast speed and easily to implement high-resolution image reconstruction algorithm to get the visual effect is often not ideal, but the visual effect is good algorithm but also time-consuming.

As mentioned earlier, the interpolation-based approach and adaptive filtering approach can reach the demand of real-time implementation. However, those easier algorithms are

always unable to reach the vision demand, and better vision algorithm would require a long time. As a consequence, it is desired to optimize those algorithms or create new algorithms to improve the efficiency and speed.

2.4.3   Suitable In For Different Situation Algorithms

The super resolution algorithms have been applied in many areas, such as the public area, medical care, or satellite. The different algorithms can only satisfy different requirements, such as real-time, reliability, and accuracy. As a result, SR technology should develop an optimal reconstruction algorithm to satisfy the multiple situations.

Chapter 3

Image Superresolution From Coprime Sampling

3.1 Theory Properties For Coprime Sampling

The coprime sampling process $x_c(t)$ with two sub-Nyquist samplers,whose sampleing spacing are MT and NT, respectively. M and N are coprime integers and $M < N$. 1/T Hz is the Nyquist rate for a bandlimited process, i.e. $1/T = 2f_{max}$, f_{max} being the maximum frequency. Then, the two sampled signals can be expressed as

$$x_1[n_1] = x[Mn_1] = X(Mn_1 T_s)$$

$$x_2[n_2] = x[Mn_2] = X(Mn_2 T_s)$$

Sampling structure are shown below.
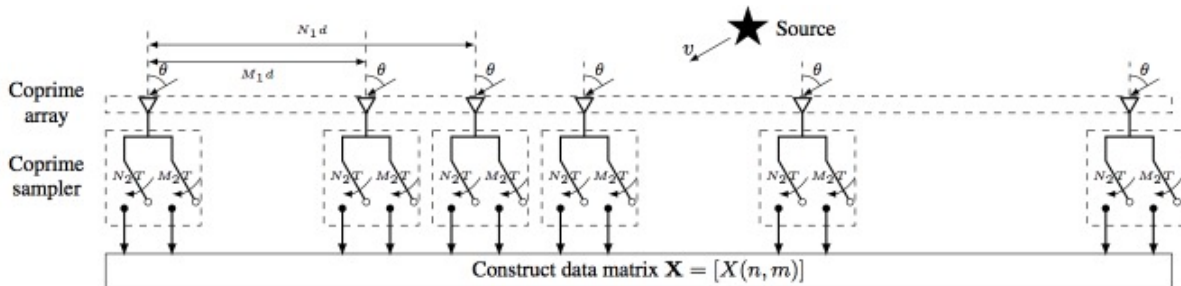
Fig. 3.1 Structure of coprime sampling

$x(Mn_1)$ and $x(Nn_2)$ is from the first and the second sampler. ifwe set the difference between those two samplers

$$k = Mn_1 - Nn_2$$

It is described in [6], that due to the corporality of M and N, k can reach to any integers among the range of $0 \leq k \leq MN - 1$, if n_1 and n_2 in the ranges $0 < n1 < 2N1$ and $0 < n2 < M1$. There will be some missing legs in the region of $-MN + 1 < k < 0$. However, the missed legs is able to obtained from the conjugation of the positive symmetric counterparts. As a result, the entries R(k) can be obtained, for k = -MN+1, ,MN-1. Considering that, the equation of $k = Mn_1 - Nn_2$ can be rewritten as $k = M(n_1 + Nl) - N(n_2 + Ml)$ for any integer l.

The autocorrelation plays a significant role in the analysis of signals and systems. The autocorrelation function of a random signal illustrates the corresponding dependence of the sample's values at a time and the sample's values at another time. As a consequence, the estimation of full-rank Toeplitz correlation matrix can be described as

$$\mathbf{R}_{\text{est}} = \begin{pmatrix} R_{\text{est}}(0) & R_{\text{est}}(-1) & \cdots & R_{\text{est}}(-MN+1) \\ R_{\text{est}}(1) & R_{\text{est}}(0) & \cdots & R_{\text{est}}(-MN+2) \\ \vdots & \vdots & \cdots & \vdots \\ R_{\text{est}}(MN-1) & R_{\text{est}}(MN-2) & \cdots & R_{\text{est}}(0) \end{pmatrix}$$

where, R_{est} is illustrated as

$$R_{\text{est}}(k) = \begin{cases} \dfrac{1}{L} \displaystyle\sum_{l=0}^{L-1} x[M(n_1 + Nl)]x^*[N(n_2 + Ml)], k \in [0, MN - 1] \\ R_{\text{est}}^*(-k), k \in [-MN + 1, 0), \end{cases}$$

It should be noticed in here that

$$n_1 \in [0, 2N - 1], \; n_2 \in [0, M - 1]$$

and L is the amount of average time domain blocks, l is a non-negative integer.

For coprime sampling, the total samples collected from these two sampler are M+N in the period of 2MT seconds, but the average sampling rate can be estimated as

23

$$f_{s,sample} = \frac{M+N}{\text{MNT}} = \frac{1}{MT} + \frac{1}{NT} < \frac{1}{T}$$

From this coprime sampling equation, we can get that the sampling rate of coprime sampling is much smaller than the conventional Nyquist sampling rate of 1/T. The sampling rate of this two samplers is fs/M and fs/N respectively, but this algorithm is able to estimate up to MN frequency in the spectrum domain, with the frequency resolution up to fs/(MN).

If we set N_1 and N_2 as the larger numbers, the average sampling rate f_s can be smaller. As a consequence, we can make this conclusion that with N_1 and N_2 becoming larger, the density of power spectrum goes narrower. In another words, the spectrum can be used more efficiently.

3.1.1 Generalized coprime sampling

As it describe befor, the coprime sampling structure can be used to estimate the low Nyquist sampling rates. Therefore, the detectable frequencies will increase if the value of M and N increases. However, along with the increase of M and N the latency time(which is around MNLT) will also increases. Meanwhile, for the constant data, there will be less samples as well. As a result, the performace of spectrum estimation maybe inaccuracy, or even incorrect.

A generalized coprime sampling technique is concerned by P. P. Vaidyanathan[6] with O(M + pN) samples to estimate O(pMN) virtual samples. The resolution becomes better along with the increases of p. The latency time, meanwhile, slightly increases with p, this difference becomes negligible along with the increase of L.

Considering this, an integer factor p is employed to achieve more lags that convential coprime sampling. In generalized coprime sampling methods, we use pN samples rather than just 2N samples to estimate the correlation matrix. For the second sampler, it still use M sampes. In this situation, the computable lags can be written as following set,

$$\mathbb{K} = \{k | k = Mn_1 - Nn_2, 0 \le n_1 \le pN - 1, 0 \le n_2 \le M - 1\}$$

It is clear that for any different integer p, we are able to compute a different length of

set K. The Fig5 shown the valid lags for different value of p (2-4 in the figures).
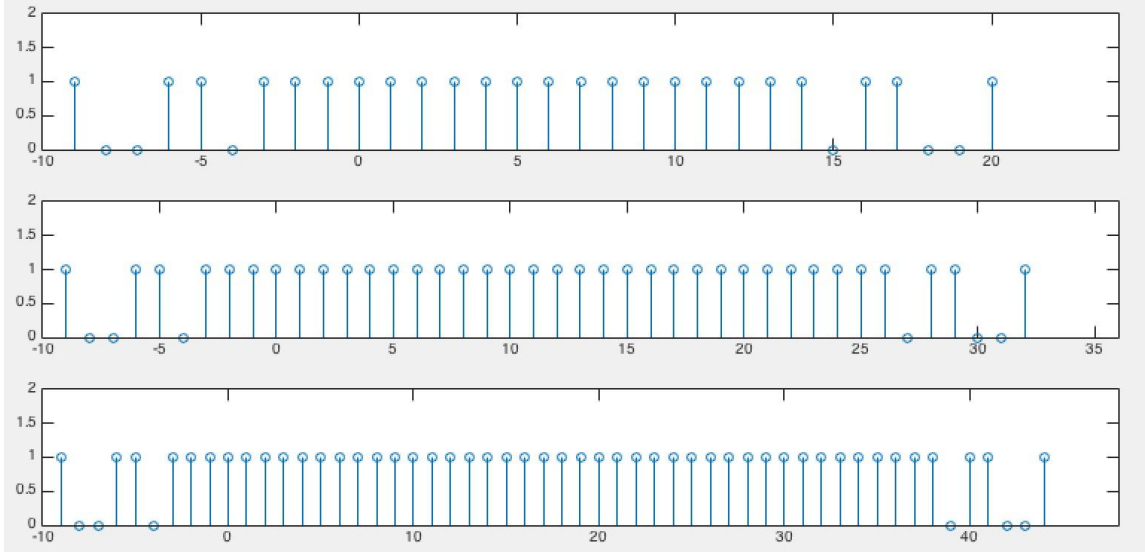
Fig. 3.2 The set K with different values of p (Top:p=2, Middle:p=3, Bottom:p=4; M = 4, N = 3 and 1: Valid lags, 0: Missed lags)

So that, the set K can compute all the intergers in the region of $[0, (p-1)MN + N + 1]$.

For this concern, the auto-correlation matrix R_{est} can be rewritten as ,

$$
\tilde{R}_{est}(k) = \begin{cases} \dfrac{1}{L} \sum_{l=0}^{L-1} x[M(n_1 + Nl)]x^*[N(n_2 + Ml)], k \in [0, (p-1)MN + N - 1] \\ \tilde{R}_{est}^*(-k), k \in [-(p-1)MN - N + 1, 0), \end{cases}
$$

where $0 < n_1 < pN - 1$ and $0 < n_2 < M - 1$.

In the case of p = 2, it becomes the conventional coprime sampling which has been discussed before. We can get in here, that the conventional coprime sampling case can be treated as a specific case in this general copriem sampling. Thus, we can summarize the generalized coprime sampling as below:

i. The maximum sampling rate used in sub-Nyquist sampler is the larger value of f_s/M and f_s/N.

ii. The maximum estimated frequency in the spectrum is $(p-1)MN + N - 1$.

iii. The frequency resolution can be estimated reach to $f_s/[(p-1)MN]$. The resolution is improved by a factor of p-1.

Consequently, if the value of L is large enough, increasing the value of p can reach a good performance in spectrum estimation rather than increasing the value of M and N, which is mentioned before in conventional coprime sampling.
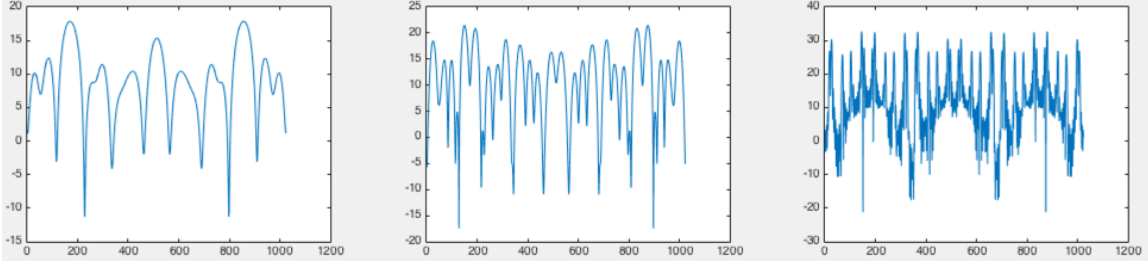
Fig. 3.3 Estimated spectrum for different values of p. (left:p=2, middle:p=5, right:p=20)

3.1.2   Music algorithm

Multiple Signal Classification(MUSIC) algorithm is first presented by R.O.Schmidt in 1979. The idea of this algorithm is to do the eigendecomposition in the covariance matrix of a signal or array . The sub-space of the corresponding signals components and the noise sub-space of signal component phase is computed. The MUSIC algorithm is able to estimate the DOA with smaller SNR(Signal-to-Noise Ratio),

The idea of MUSIC is to do the spectrum estimation for a signal or an correlation matrix in the eigenspace. In this algorithm, it have a previous assumption that there are p complex components and this signal contains the Gussian white noise. Thus, for a MxM correlation matrix Rx, the eigendecomposition has be used. If the eigenvalues are arranged in the descend order, the first p corresponding eigenvectors compose the signal sub-space. The reminding M-p eigenvectors, which is only the noise, span in the orthogonal space. [MARK] It should be mentioned in here is that the MUSIC algorithm can be equal to Pisarenko harmonic decomposition if M=p+1.

The frequency estimation of this algorithm can be written as

$$P_{MU}(e^{jw}) = \frac{1}{\sum_{i=p+1}^{M} |e^H V_i|^2}$$

where v_i are the noise eigenvectors and

$$e = [\ 1,\ e^{j\omega},\ e^{j2\omega},\ e^{j3\omega}...\ e^{j(M-1)\omega}]^T$$
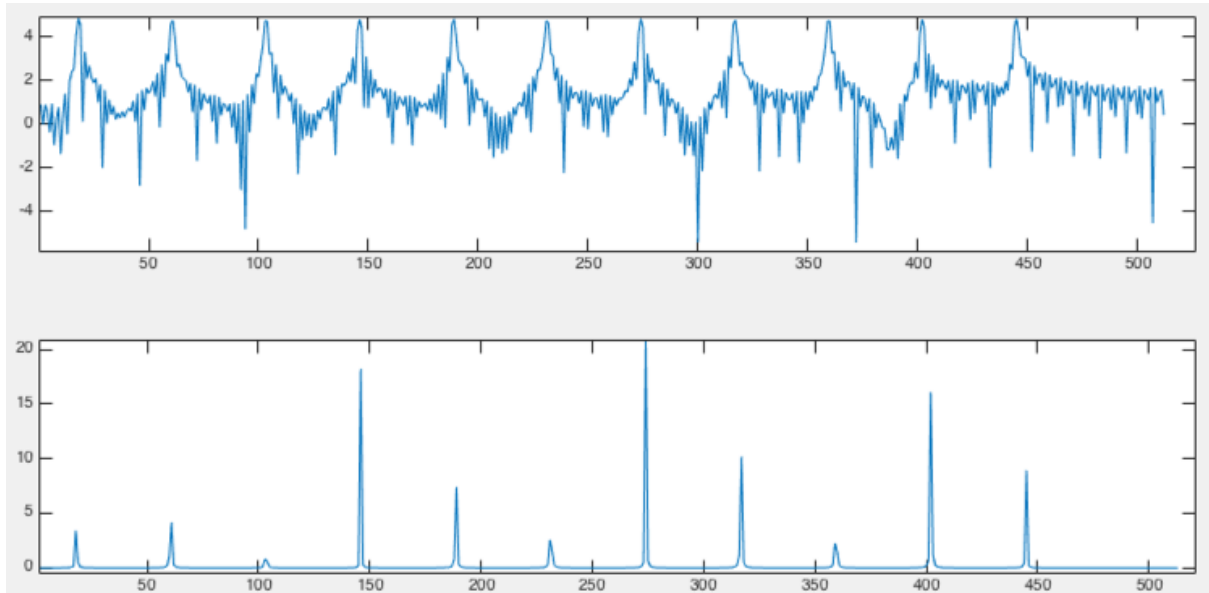
Fig. 3.4 Comparision of FFT and MUSIC algorithm (top: DFT, bottom: MUSIC)

This figure illustrates the spectrum of DFT and MUSIC algorithm. We can see clearly from this figure that the location with the largest peak provide the frequency estimation of the signal coponents. In addition, zeros are not presented in here, due to the assupmption that many components would be added together. Thus, the location of peak has be searched and estimated by computation. In the presence of noise, MUSIC provides a better algorithm in the process of picking peaks compared with DFT spectrum, bacuase MUSIC algorithm has ignore the noise during its process. However, it requires a previous knowledge that thenumber of components already known in advance.

Fot the MUSIC algorithm, the higher frequency components can be estimated higher than one sample. That is because it estimation function as shown above is able to process any frequency components, which is one form of superresolution. The main problem of MUSIC algorithm is that the number of frequency components should be known in advance, which means it is unable to applied to most general cases.

3.1.3 Co-prime sensor arrays (CSAs)

Co-prime sensor arrays (CSAs) refer to a two linear subarrays which is down-sampled by coprime factors. This non-uniform array requires less sensor compared with the uniform sensor arrays(USA) of the same aperture. However, the peak side lobe in the CSA is far higher that the peak side lobe in the USA. The appearance of side lobe in such techniques often are undesirable in array beam pattern. It is proposed to produce the non-uniform array by combining those two ULAs. It requires fewer sensor than ULA within the same aperture.

The conventional beam-forming is performed seperately in each subarray. The total beam pattern can be obtained by multiplying the two beam patterns. Its resolution, meanwhile, can reach the same dimension of a fully sampled ULA with MN elements. In the meantime, the grating lobes will not appear in the same locations, when M and N are coprime. As a result, the production of beam pattern does not have grating lobes, as the followed figure shown. The samples from MN decrease to (M+N-1), which means a significant saving the complicity, and computation demand.
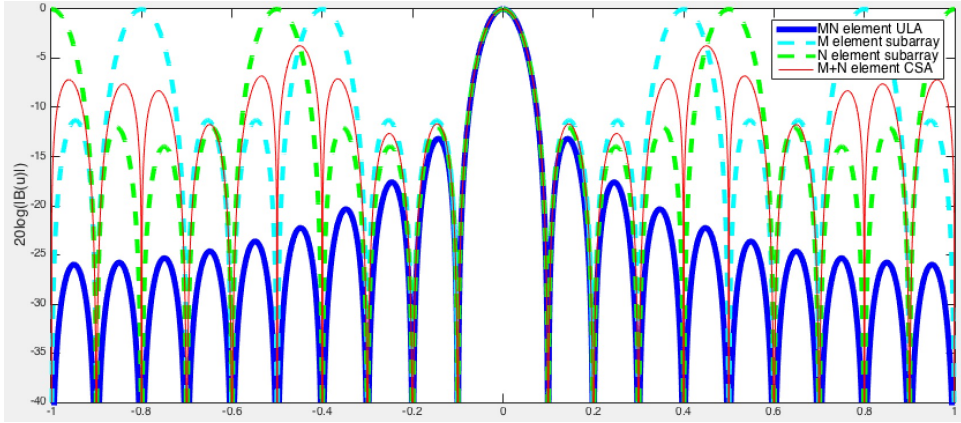
The beam-patterns of those two conventional beam-formed subarrays are described as the following equations

$$B_{M,N}(u) = \frac{1}{M} \frac{\sin\left(\frac{\pi MN}{2} u\right)}{\sin\left(\frac{\pi N}{2} u\right)}$$

$$B_{N,M}(u) = \frac{1}{N} \frac{\sin\left(\frac{\pi MN}{2} u\right)}{\sin\left(\frac{\pi M}{2} u\right)}$$

where, u = $\cos(\theta)$.

Fig. 3.5 The beam pattern of ULA(blue), M elements subarray(cyan), N elements subarray(green), and the combined M+N elements CSA

Both subarrays beam patterns (cyan and green dash line) are start from the bradside (u = cos($\pi/2$) = 0). In spite of the same resolution that the multiplication of those two beam pattern achived, the peak lobe of CSA beam pattern is higher than the ULA with MN elements. It is proposed by Vaidyanathan and Pal [10] that extending each subarray is able to reduce the high side lobes of CSA. The width of grating lobe in the subarray beam patterns can also be reduced. As a result, the overlap between two grating lobes can be alleviated.

3.2   Image Reconstruction

The implementation of this algorithm is first down sampled a high resolution image to two LR images with the coprime down sampling rate M and N respectively. To keep the high resolution information, aliasing is kept in here, as illustrated in followed figure. The purpose is to recovery the original images. In another words, it is try to separate the high frequency components from the aliasing area.
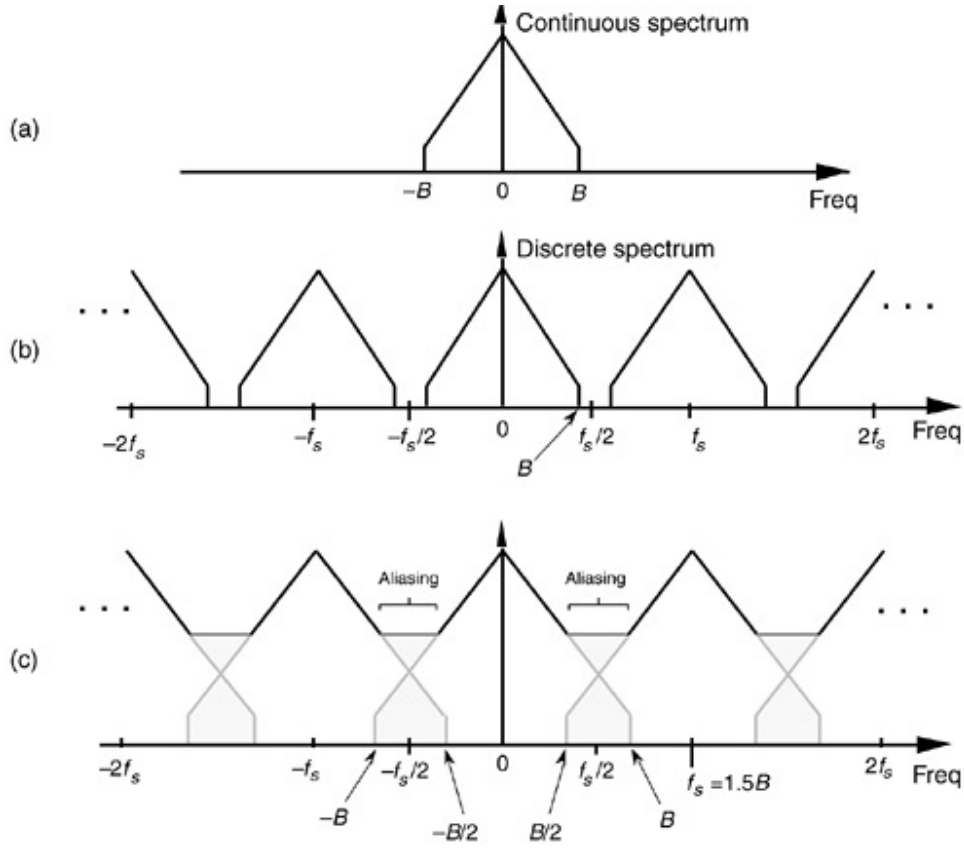
Fig. 3.6 The appearance of aliasing when the signal is down-sampled.

The followed figure shows an example with 12 x12 image blocks. After $D_{I=2}^{n=3}$ break down, a down sampled 6 x6 image is get with third phase u_i, which is represented as the black blocks in the middle. And second image is break down by $D_{J=2}^{m=1}$, and a 4 x4 image u_m is illustrated with gray blocks.

The $u_{n,j}$ is then get from u_n which is down sampled by $D_{J=3}^{j=4}$. And $u_{m,i}$ will be get from u_m which is down sampled by $D_{I=3}^{i=3}$. It is clear that $u_{n,j}$ is same with $u_{m,i}$. If I and J are coprime integer ($I \neq uJ$), for any down sampling rate I, J and any phase n,m, there have and only have one common sub-frame phase, which is satiated $u_{n,j} = u_{m,i}$, as shown in the following equation

$$u_{n,j} = D_J^j D_I^n u = D_I^i D_J^m u = u_{m,i}.$$

This sampling method is called diversity sampling algorithm.
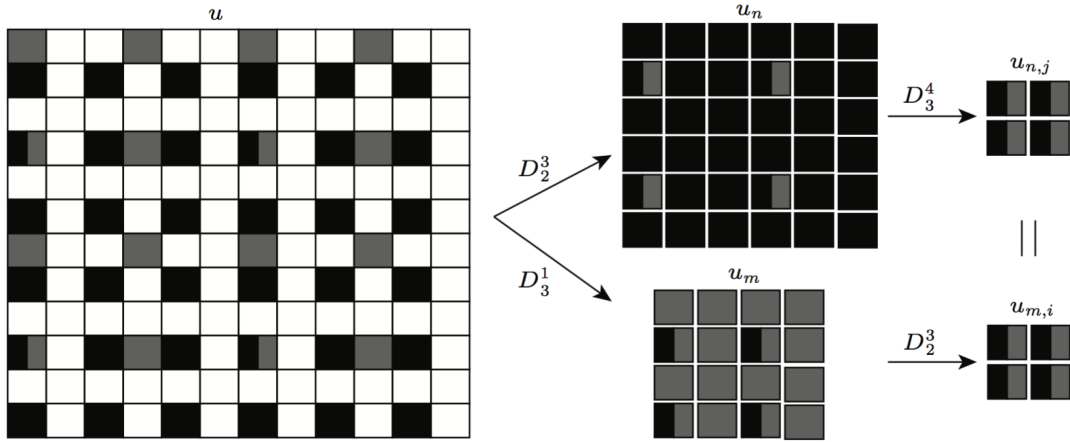
Fig. 3.7 The illustration of sampling rate diversity

Let us now define an image x[k] of size N. In here, we only deal with one dimension images, as it perform the same work for two dimensional images with extension. It is assume that the image is bandlimited to the interval (-pi , pi). As a sequence, we can get the DFT of the image, which can be written as:

$$X[n] = \sum_{k=0}^{N-1} x[k] e^{-j2\pi kn/N}$$

Meanwhile, the inverse DFT can be express as:

$$x[k] = \sum_{n=0}^{N-1} X[n] e^{j2\pi kn/N}$$

We suppose that we have two down sampled images x1[k] and x2[k], which have the size of N1 and N2 respectively. Moreover, we assume that both images do not lose generality, and N ¡ N1 ¡ N2. Therefore, two DFTs are given by:

$$X_1[l] = \sum_{k=0}^{N_1-1} x_1[k] e^{-j2\pi kl/N_1}$$

$$X_2[l] = \sum_{k=0}^{N_2-1} x_2[k] e^{-j2\pi kl/N_2}$$

31

As the two images N_1 and N_2 is down-sampled from N, so that N = N*N1 = MN2, where N and M are coprime integer. In another words, the sequence of x1[k] and x2[k] are the subsequence of x[k]. Thus, x1[k] = x[Nk], and x2[k] = x[Mk]. Therefore, with the combination, we can get

$$X_1[l] = \sum_{k=0}^{N_1-1} \sum_{n=0}^{N-1} X[n] e^{j2\pi\alpha_1 kn/N} e^{-j2\pi kl/N_1}$$

$$= \sum_{n=0}^{N-1} X[n] \sum_{k=0}^{N_1-1} e^{j2\pi\alpha_1 \frac{k}{N}(n-l)}.$$

$$X_2[l] = \sum_{k=0}^{N_2-1} \sum_{n=0}^{N-1} X[n] e^{j2\pi\alpha_2 kn/N} e^{-j2\pi kl/N_2}$$

$$= \sum_{n=0}^{N-1} X[n] \sum_{k=0}^{N_2-1} e^{j2\pi\alpha_2 \frac{k}{N}(n-l)}.$$

Since the inner sum is 0 for n not equal to rNi + l, and the image is bandlimited, the equation then can be written as

$$X_1[l] = \sum_{r=0}^{\alpha_1-1} X[rN_1 + l]$$

$$X_2[l] = \sum_{r=0}^{\alpha_2-1} X[rN_2 + l]$$

Then, we can estimate the frequency components for each blocks. Here is the example with sampling rate N=2 and M = 3 as below.
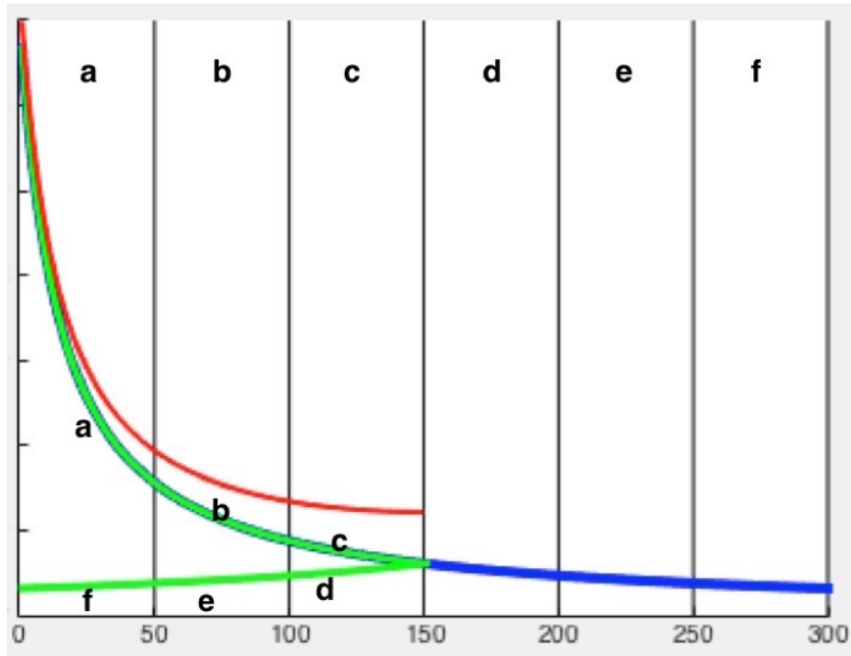
Fig. 3.8 Frequency domain with down sampling rate is 2

$$Xn1 = a + f;$$
$$Xn2 = b + e;$$
$$Xn3 = c + d.$$
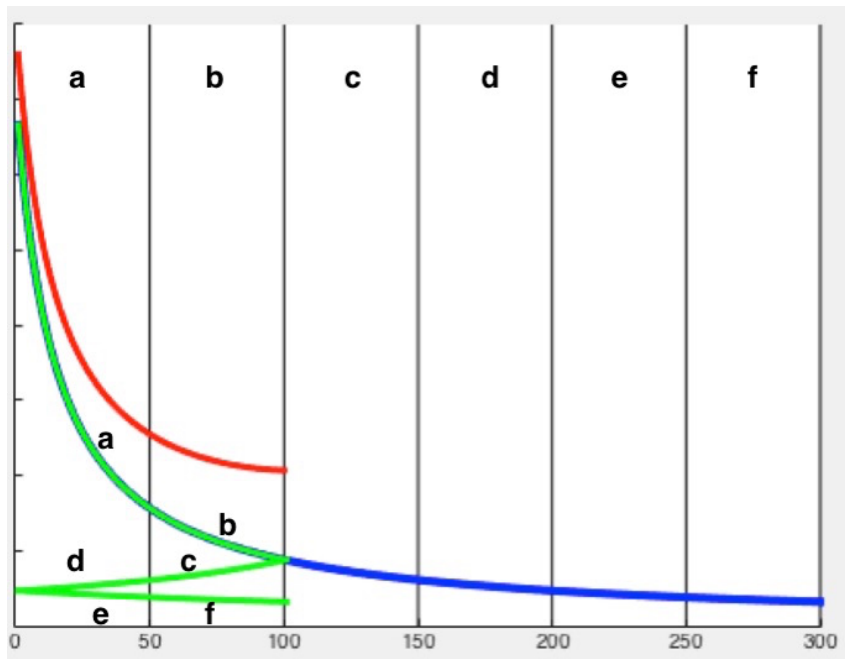

Fig. 3.9 Frequency domain with down sampling rate is 3

$$Xm1 = a + d + e;$$

$$Xm2 = b + c + f;$$

For the real image, the high frequency components are usually in a small number. Therefore, the highest frequency block f is assumed to be zero. We can estimate other blocks with the iteration from e=0.

$$a = Xn1;$$

$$d = Xm1 - Xn1;$$

$$c = Xn3 - d;$$

$$b = Xm2 - c;$$

$$e = Xn2 - b.$$

After the estimation of each frequency component block, we can reconstruct the image by taking the inverse DFT.

## 3.3 Enhancement Using Adaptive Steering Kernel Regression

According to the imaging model, the initial high-resolution image contains noise and blur, thus it requires to use the image enhancement algorithms to get the final high resolution image U[19]. The image restoration method based on Adaptive Steering Kernel Regression considers spatial distance and grey-scale distance, which is a local nonlinear combination of data and has good properties in image restoration process. An improved image restoration algorithm based on control kernel regression is used to adaptively adjust the weights through anisotropic distance. For any point in the image $pi = [xi, yi]$, the Adaptive Steering Kernel can be written as

$$K\left(p_l - p_i\right)$$
$$= \sqrt{\det(C_l)} \exp\{-(p_l - p_i)^{\mathrm{T}} C_l (p_l - p_i)\}$$

where l is the neighbourhood pixel in the control window Wl of π and C_l is the local covariance matrix of the image. C_l determines the extension, rotation and scaling of the

kernel.The covariance matrix C_l is used to determine whether the pixel is a smooth or an edge-point and adaptive adjust the control kernel.

It is performed by a basic point of the improvement in the method always a linear combination a local polynomial regression to estimate core independent of the local data[19]. Therefore, the analysis elegant, but also a relatively easy way, and the combined attractive asymptotic properties, still a problem because of the inherent limitations of linear local action on the data. As well as the data adaptive kernel regression method, the position of the sample to the emission characteristics of these samples as well as the density denpends. Accordingly, the effective size and shape of kernel regression to the local image characteristics, such as configuration, such edge. This attribute is shown in the following figure:

Elongate   Rotate   Scale
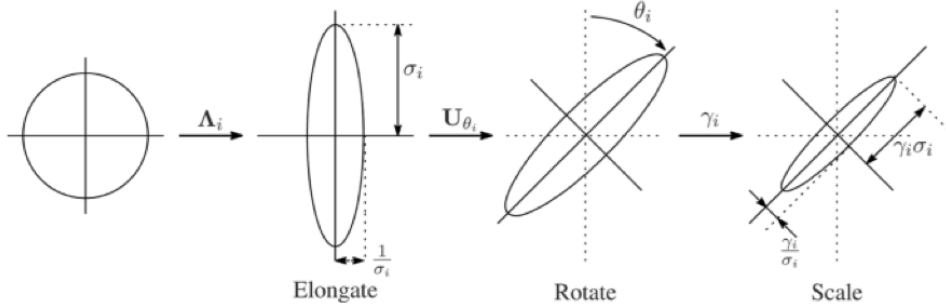
Fig. 3.10 The illustration of the effects of the steering matrix and the component on the size and shape of the regression kernel

where the classical and adaptive kernel shapes are compared in the presence of edges. The data fit kernel regression is constructed as an optimization problem.

$$
\min_{\{\boldsymbol{\beta}_n\}} \sum_{i=1}^{P} \Big[y_i - \beta_0 - \boldsymbol{\beta}_1^T (\mathbf{x}_i - \mathbf{x})
$$
$$
- \boldsymbol{\beta}_2^T \operatorname{vech} \big\{ (\mathbf{x}_i - \mathbf{x})(\mathbf{x}_i - \mathbf{x})^T \big\} - \cdots \Big]^2
$$
$$
\cdot K_{\text{adapt}}(\mathbf{x}_i - \mathbf{x}, y_i - y)
$$

where the data-adapted kernel K(adapt) function now depends on the spatial sample locations $X_i S$ and density, as well as the radiometric values y_i of the data[19].

On the previous parametric framework, and further proposed a method to filter the next shot idea. In particular, measuring the function of the local slope estimates between adjacent values suggests the effectiveness of the operation and observed to measure each weight is used to estimate[19]. If the pixel is located near the edge, for example, then the pixel of the boundary have a much stronger impact on the same side of the filtrate. It uses some kind of insight into the mind of the initial image estimate the slope gradient regression method estimates the initial two-step approach is proposed classics secondary core that is being carried out. Next, this estimate is used to determine the dominant direction of the image gradient regions.

A second stage filter, this orientation information is used instead in the direction of extending "manipulation" local core results contour adaptively oval edge structure to impart distribution. These nuclei together to remove noise is performed more strongly to strong local conservation results through them rather than the edge of the details of the final output. In other words, the core adapted data takes the form

$$K_{\mathrm{adapt}}(\mathbf{x}_i - \mathbf{x}, y_i - y) \equiv K_{\mathbf{H}_i^{\mathrm{steer}}}(\mathbf{x}_i - \mathbf{x})$$

where H_i are now the data-dependent full matrices which we call steering matrices. We define them as

$$\mathbf{H}_i^{\mathrm{steer}} = h\mu_i \mathbf{C}_i^{-\frac{1}{2}}$$

where Cs are (symmetric) covariance matrices accoding to differences in the local gray-values. Along the local edge, the choose of C_{is} will effectively impact the kernel functions, as shown in the following figure.

(a)   (b)

36
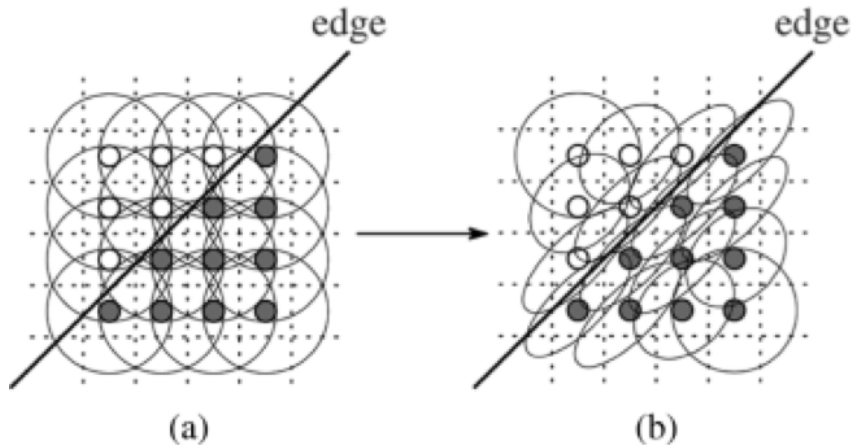
Fig. 3.11 The kernel expands in the uniformly sampled data set. (A) The core in the classical method depends on the sample density. (B) The kernel of the data fit is elongated relative to the edge.

It should be noted that even if we choose large to have a strong denoising effect. Otherwise, undesirable blurring effects would be modulated at the edges by appropriately chosen. For example, by using such a steering matrix, once the Gaussian kernel is determined, the steering kernel then can be writtten as

$$K_{\mathbf{H}_i^{\text{steer}}}(\mathbf{x}_i - \mathbf{x}) = \frac{\sqrt{\det(\mathbf{C}_i)}}{2\pi h^2 \mu_i^2} \exp\left\{-\frac{(\mathbf{x}_i-\mathbf{x})^T \mathbf{C}_i (\mathbf{x}_i-\mathbf{x})}{2h^2\mu_i^2}\right\}$$

The local edge structure is then associated with a gradient covariance ie equivalently, a local dominant orientation, where the original estimation of the covariance matrix can be organized as follows:

$$\hat{\mathbf{C}}_i \approx \begin{bmatrix} \sum_{\mathbf{x}_j \in w_i} z_{x_1}(\mathbf{x}_j) z_{x_1}(\mathbf{x}_j) & \sum_{\mathbf{x}_j \in w_i} z_{x_1}(\mathbf{x}_j) z_{x_2}(\mathbf{x}_j) \\ \sum_{\mathbf{x}_i \in w_i} z_{x_1}(\mathbf{x}_j) z_{x_2}(\mathbf{x}_j) & \sum_{\mathbf{x}_i \in w_i} z_{x_2}(\mathbf{x}_j) z_{x_2}(\mathbf{x}_j) \end{bmatrix}$$

where $Z_{x1}()$ and $Z_{x2}()$ are the first derivatives along x1 and x2 directions and Wi is a local analysis window around the position of interest.

The direction of the dominant region of the gradient is related to the eigenvectors of the estimated matrix to the next. The $Z_1()$ and $Z_2()$ is Yi pixel value gradient that depends on. Because it depends on the selection of the localized gradient kernel, therefore, the proposed data is equipped with a "corresponding" kernel of a method of forming a local "non-linear" coupling of the data.

This method is simple, but has a good immunity to noise, estimation of the resulting covariance often may be the rank deficiency or unstable state, care must be taken when hajiyi obtain the reciprocal of the estimated treatment directly. At this time, it can be obtained by using the estimated covariance stable diagonal loading or normalization. We efficient multi estimating the local orientation satisfying the requirements of this problem, we propose a technical scale[19]. Through knowledge of the above, in this paper, we use a parameterized how to design a matrix adjustment. For convenience in the form of a

covariance matrix, we have three components (equivalent eigenvalue decomposition), and then decomposed into:

$$\mathbf{C}_i = \gamma_i \mathbf{U}_{\theta_i} \mathbf{\Lambda}_i \mathbf{U}_{\theta_i}^T,$$

$$\mathbf{U}_{\theta_i} = \begin{bmatrix} \cos\theta_i & \sin\theta_i \\ -\sin\theta_i & \cos\theta_i \end{bmatrix}$$

$$\mathbf{\Lambda}_i = \begin{bmatrix} \sigma_i & 0 \\ 0 & \sigma_i^{-1} \end{bmatrix}$$

where U is the rotation matrix, A is stretched matrix. Covariance matrix is now given by the respective scaling, rotation, and height parameters of three parameters, , and .

This figure shows how these parameters affect the expansion of the kernel. First, it is extended by a circular core matrix kidney child, given the long and the small axis of the Sigma half. Second, slender kernel matrix U_theta is rotated[20]. Finally, it is scaled by scaling the kernel parameter . Scaling, rotation and height parameters are defined as follows. The dominant gradient direction of a local area is a specific vector corresponding to a specific value other than 0 is the smallest of the local gradient matrix arranged in the following forms:

$$\mathbf{G}_i = \begin{bmatrix} \vdots & \vdots \\ z_{x_1}(\mathbf{x}_j) & z_{x_2}(\mathbf{x}_j) \\ \vdots & \vdots \end{bmatrix} = \mathbf{U}_i \mathbf{S}_i \mathbf{V}_i^T, \quad \mathbf{x}_j \in w_i$$

where cleavage specificity value of $U_i S_i V_i$ gastrointestinal tract, a 2 2 diagonal matrix that represents the energy in the dominant direction of the Si. Then, the second column of the 2x2 orthogonal matrix Vi, $v_2 = [v_1, v_2]^T$, defines the dominant orientation angle theta

$$\theta_i = \arctan\left(\frac{\nu_1}{\nu_2}\right)$$

That is specifically corresponding to the minimum non-zero singular values of the gastrointestinal tract vector shows the dominant direction of the local gradient field. Elongation may be selected corresponding to the energy of the parameter sigma dominant gradient direction

$$\sigma_i = \frac{s_1 + \lambda'}{s_2 + \lambda'}, \quad \lambda' \geq 0$$

where sigma is a regularization parameter for the kernel elongation. The scaling parameter gamma is defined by

$$\gamma_i = \left(\frac{s_1 s_2 + \lambda''}{M} \right)^{\frac{1}{2}}$$

where sigma is the parameter for the kernel elongation, which describes the effect of the noise, and the ratio of degeneration.
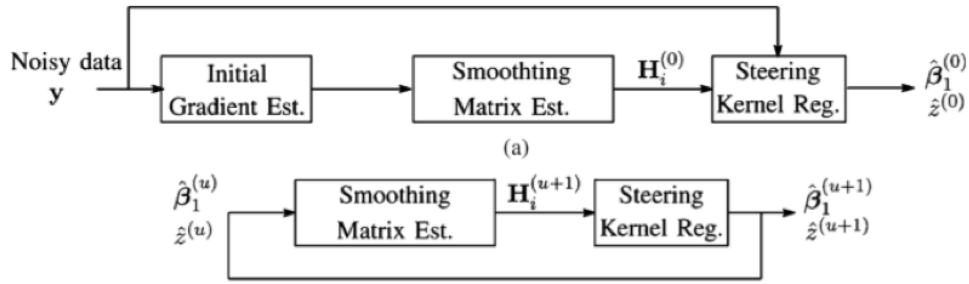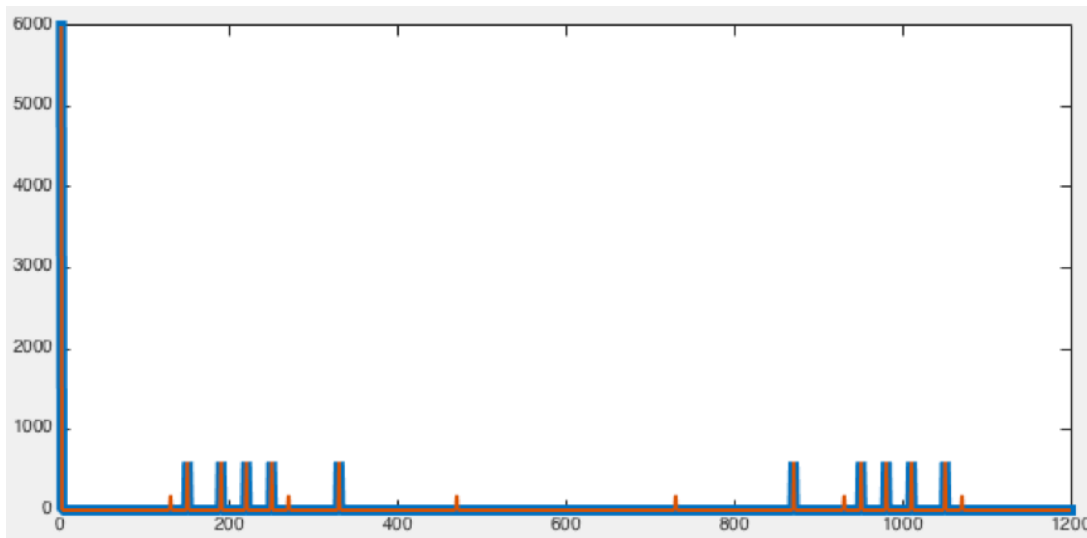

Fig. 3.12 Block of repeating steering kernel regression. (A) Initialization. (B) Iteration

Chapter 4

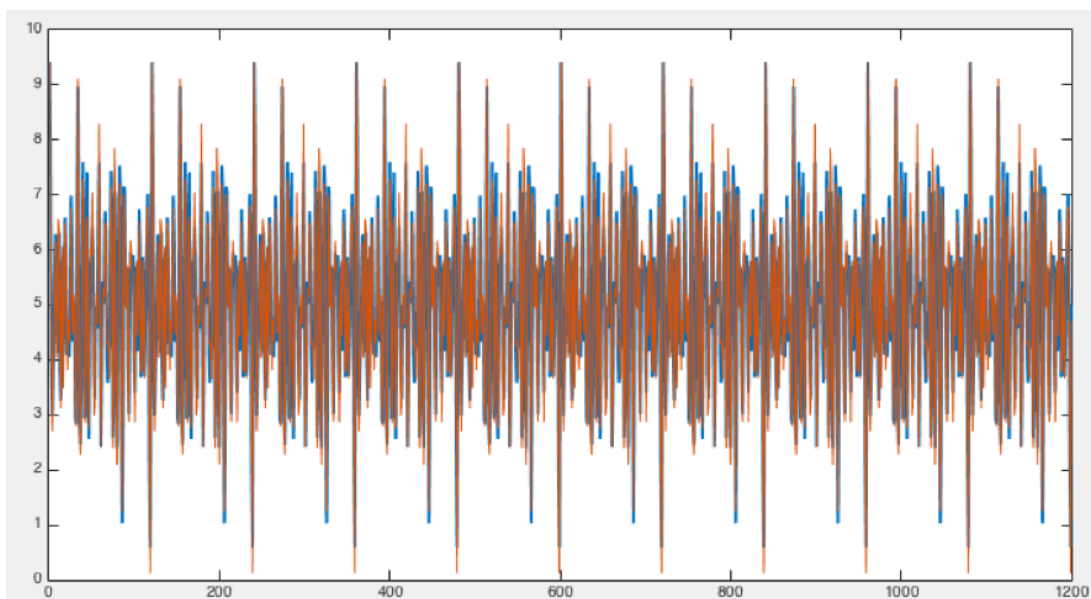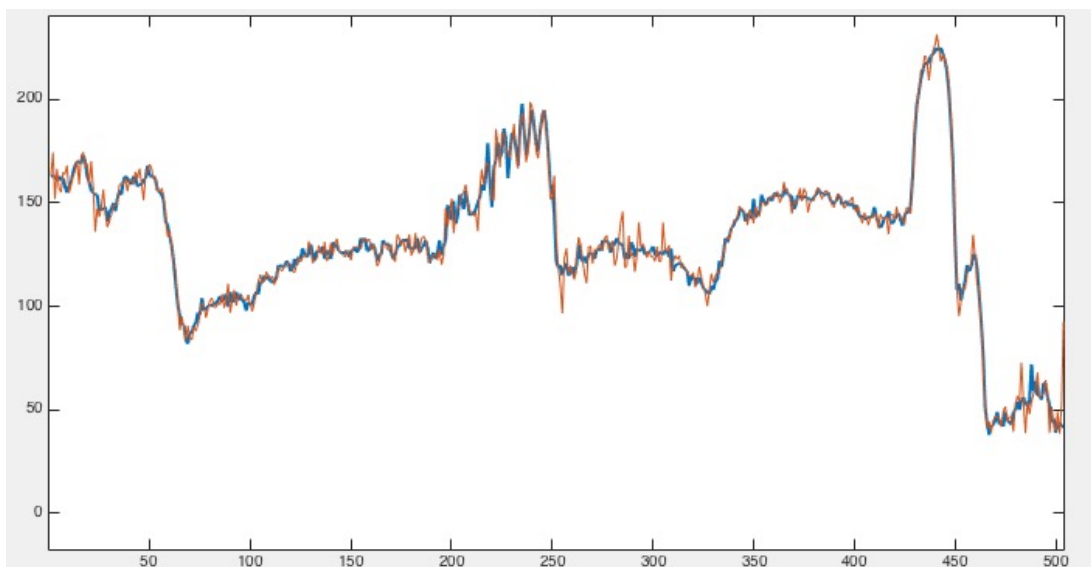# Experimental Results

4.1   1D Signal Recovery

A multiple frequency sinusoidal signal is taken as the example, with the frequency is [150, 190, 220, 250,330].

Fig. 4.1 Frequency domain estimation (blue: original signal; red estimated signal)

Fig. 4.2 Restructed 1D Signal (Blue: original signal; Red: resorted signal)

Fig. 4.3 Restored signal (Blue: original signal; Red: resorted signal)

4.2   2D Image with coprime sampling

The image with coprime sampling rate N =2 and M =3 has be evaluated in here. The orignal image X is 256x256 pixels image. It will down sampled with 2 and 3, and then reconstruct it, which is shown in the followed figures.

Fig. 4.4 Down sampling rate with 2(left) and 3 (right)

Fig. 4.5 Super resolution by the method of Coprime sampling

This figure shows the reconstructed result of method NEDI (New Edge-Directed Interpolation) from the 128x128 pixels image, from the 128x128 pixels image, which is down sampled from 256x256 pixels image.

Fig. 4.6 Super resolution by the method of NEDI

This figure shows the reconstructed result of method ScSR (Super-Resolution Via Sparse Representation) from the 128x128 pixels image, which is down sampled from 256x256 pixels image.
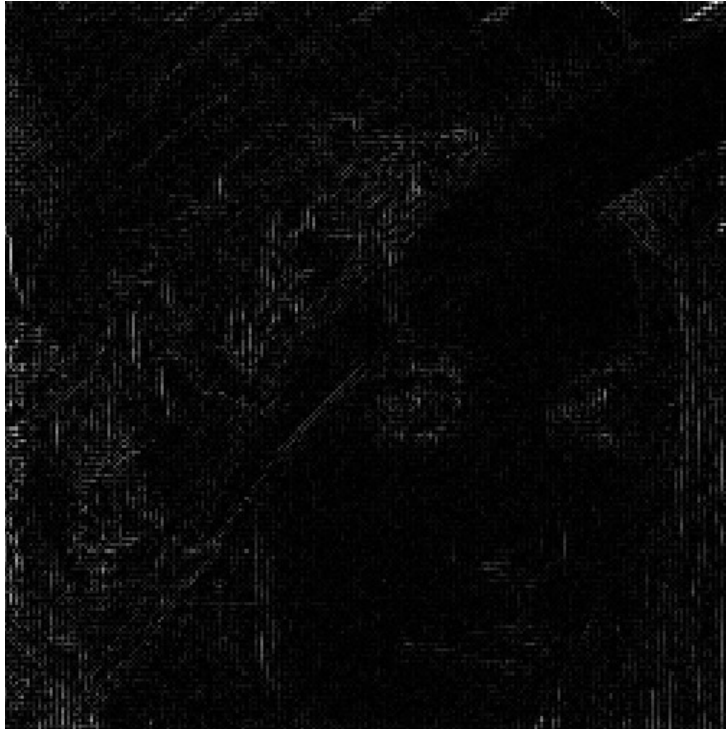
4.3 The Comparison of Each Pixel

To find more detail difference between those methods, the comparisons of each pixel are made, which is shown in the followed figures. the illumination of each pixel refers to the difference between the original image. With the comparison of those three figures, the coprime sampling has a better feature to detect the high frequency components, as the pixel value in the high frequency parts are lower that other two methods. However, some undesired noise is introduced, especially for the low frequency parts. Therefore, the algorithm should be improved and optimized. Meanwhile, the after process is also could be used to improve the reconstructed quality.
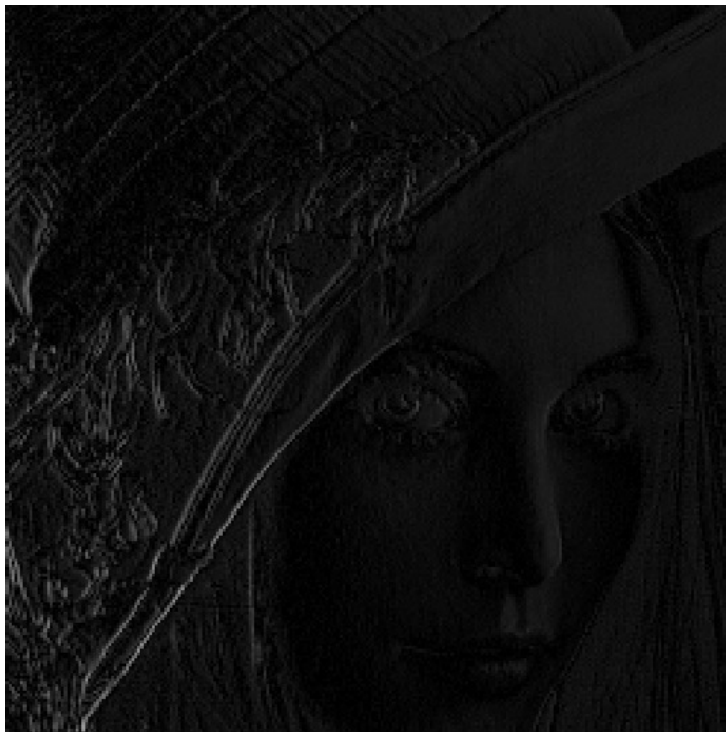

Fig. 4.8 The comparision of the method of coprime sampling with orignal image

Fig. 4.9 The comparision of the method of NEDI with orignal image

Fig. 4.10 The comparision of the method of SCSR with orignal image

4.4 The Comparison of Time and PSNR

In order to compare the reconstructed results of each algorithm objectively, we choose reconstruction time and peak signal to noise ratio to carry out the quantitative evaluation of reconstruction.The reconstruction time reflects the overall computational efficiency of the algorithm, and the PSNR value reflects the similarity of the gray information between the reconstructed image and the HR image. The larger the PSNR value, the more similar the reconstructed image and the HR image are in structure and gray information.

The comparison results are listed in the followed table. The results of the table show that Bicubic interpolation has the shortest reconstruction time but the worst effect. The sparse learning method is more effective than the Bicubic interpolation method, because the sparse learning method takes the training time of the sample into consideration, and its reconstruction time is obviously larger than other methods. For the coprime sampling method developed in this paper, the PSNR index of the algorithm is obviously improved, and the computing efficiency is also improved obviously.

Method	Time /s	PSNR(dB)
Bicubic	0.0132	20.1873
ScSR	14.637	29.5246
NEDI	2.6023	24.6342
Co-prime Sampling	4.6211	25.6324

Table. 1. Comparison for each method based on running time(s) and PSNR(dB).

Chapter 5

Conclusion

This paper presented the methods of super resolution and evaluate coprime sampling reconstruction method. Experimental results are demonstrated to make the comparison. Meanwhile, the after-process method is also developed to evaluate the effect of blurring and noising. With the compare of results, it shows that the coprime sampling method can reach a desired performance in the computation speed and PSNR, when compare those index with SCSR (Super-Resolution Sparse Representation) and NEDI(New Edge-Directed Interpolation).The coprime sampling array can greatly detect the high frequency information and the ability of immunise from the noise.

5.1   Future Work

Although this method reached a desired result and has a good performance compared with others, additional enhancement should be developed to get a better result to increase the computation speed or the PSNR. Meanwhile, the noise still has a big impact on the recovered high resolution image. Therefore, additional after process is desired.

Bibliography

[1] PU J, ZHANG J, HUANG H. A survey of super resolution algorithms. Vol.39, No.1 2009.

[2] Sung Cheol Park, Min Kyu Park, Moon Gi Kang. "Super-Resolution Image Reconstruction: A Technical Overview".IEEE Signal Processing, Vol:20,No: 3, pp: 21-36.

[3] Si Qin, Yimin D. Zhang, and Moeness G. Amin, High-Resolution Frequency Estimation Using Generalized Coprime Sampling, Proceedings of SPIE-The International Society for Optical Engineering 9497.

[4] Chen JJ. ,Liang QL. ,Zhang BJ. ,Wu XR. . "Spectrum efficiency of nested sparse sampling and coprime sampling". 2013:47-53.

[5] Kaushallya Adhikari, John R. Buck, Kathleen E. Wage. "Beamforming with extended coprime sensor arrays". IEEE Trans. Image Processing, vol. 8, pp. 4183 - 4186, Mar. 2013.

[6] CAO Lin, ZHAO Chenglin. "Correlation detection algorithm based on co-prime sampling". TN915.6

[7] X.-G. Xia and K. Liu, A generalized Chinese remainder theorem for residue sets with errors and its application in frequency determination from multiple sensors with low sampling rates, IEEE Signal Process. Lett., vol. 12, no. 11, pp. 768771, Nov. 2005.

[8] P. P. Vaidyanathan and P. Pal, Sparse sensing with co-prime samplers and arrays, IEEE Trans. Signal Process., vol. 59, no. 2, pp. 573586, Feb. 2011.

[9] H. Ur and D. Gross, Improved resolution from subpixel shifted pictures, CVGIP: Graphical Models and Image Processing, vol. 54, pp. 181-186, Mar. 1992.[13] A. Papoulis, Generalized sampling theorem, IEEE Trans. Circuits Syst. vol. 24, pp. 652- 654, Nov. 1977

[10] S. Qin, Y. D. Zhang, and M. G. Amin, Generalized coprime array configurations for direction-of-arrival estimation, IEEE Trans. Signal Process., vol. 63, no. 6, pp. 13771390, March 2015.

[11] C.A. Segall, R. Molina, A.K. Katsaggelos, and J. Mateos, Reconstruction of high-resolution image frames from a sequence of low-resolution and compressed observations, in Proc. 2002 IEEE Int. Conf. Acoustics, Speech, and Signal Processing, vol. 2, 2002, pp. 1701-1704

[12] RAJAN D, CHAUDHURI S. Generalized interpolation and its application in super-resolution imaging [J]. Image and Vision Computing, 2001.19(13):957-969.

[13] IRANI M, PELEG S. Super resolution from image sequences [J]. ICPR-C, 1990, 90:115-120.

[14] STAR K, OSKOUI P¿ High-resolution image recovery from image-plane arrays, using convex projections[J]. Journal of the Optical SOciety of America A, 198.

[15] CHANG H, YEUNG D Y, XIONG Y. Super-resolution through neighbor embedding. IEEE Press, 2004:275-282.

[16] SCHULZ R, STEVENSON R. Extraction of high-resolution frames from video sequence[J]. IEEE Trans Image Processing, 1996, 5(6): 996-1011.

[17] Yang JC,Wright J,Huang ThS,Yi Ma, Image Super-Resolution Via Sparse ,VOL. 19, NO. 11, 2010.

[18] Li X and Orchard MT, New Edge-Directed Interpolation,IEEE Trans Image Processing, VOL. 10, NO. 10,2001.

[19] Takeda H, Farsiu S, Milanfar P, Kernel Regression for Image Processing and Reconstruction, IEEE Trans Image Processing,VOL. 16, NO. 2, 2007.

[20] Stephane M and Yu GS , Super-Resolution With Sparse Mixing Estimators, IEEE Trans Image Processing, VOL. 19, NO. 11, 2010.

[21] Filip S and Gabriel C, Super-resolution and blind deconvolution for fractional factors, Oxford University Press on behalf of The British Computer Society, Vol. 00 No. 0, 2007.